Icarus 329 (2019) 46–54

Contents lists available at ScienceDirect

Icarus

journal homepage: www.elsevier.com/locate/icarus

Lunar regolith thickness deduced from concentric craters in the CE-5 landing area

Z. Yue[a,b], K. Di[a,b,c], Z. Liu[a,*], G. Michael[d], M. Jia[a], X. Xin[a], B. Liu[a], M. Peng[a], J. Liu[e]

[a] State Key Laboratory of Remote Sensing Science, Institute of Remote Sensing and Digital Earth Chinese Academy of Sciences, Beijing 100101, China
[b] CAS Center for Excellence in Comparative Planetology, Hefei 230026, China
[c] Space Science Institute, Macau University of Science and Technology, Macau 519020, China
[d] Institute of Geological Sciences, Freie Unversitaet Berlin, Malteser Strasse 74-100, Haus D, Berlin 12249, Germany
[e] Institute of Geochemistry Chinese Academy of Sciences, Guiyang 550002, China

ARTICLE INFO

Keywords:
Lunar regolith
CE-5 landing area
Concentric craters

ABSTRACT

Lunar regolith is the layer of fragmented and unconsolidated rock material that is repeatedly stirred and overturned on the lunar surface. It can provide critical information about lunar geologic processes (e.g., impact, volcanism) and the space environment. China's Chang'E-5 (CE-5) mission, which will be launched in 2019, will land on the lunar near-side surface and return at least 2 kg of lunar regolith through surface collection and by boring a hole no < 2 m in depth. This study focuses on the depth of lunar regolith in the planned CE-5 landing area, which may be important for sampling activity and related scientific research. The traditional crater morphological method uses the dimensions of particular craters to derive the lunar regolith thickness, i.e., the lunar regolith thickness is estimated through the characterization of concentric, flat bottomed, and central mound craters. However, recent studies show that flat bottomed and central mound craters can also be formed by clustered projectiles. Therefore, only concentric craters were used to estimate the lunar regolith depth in this study, and subsequent morphological analysis indeed indicates that flat bottomed and central mound craters were primarily formed from secondary clustered impacts in this area. The precise locations and sizes of the selected concentric craters were determined from a high-resolution seamless Digital Orthophoto Map (DOM) of the CE-5 landing area, which was generated by our team using 765 selected LROC NAC images. All the concentric craters, including the inner and outer crater rims, were then mapped in the DOM. Local lunar regolith depths were derived according to the previously established relationship between lunar regolith depth and the inner and outer diameters. The results show that the lunar regolith in the area ranges from 0.74 m to 18.00 m, with a mean of 7.15 m, and is much shallower in the southeast than in other areas.

1. Introduction

Chang'E-5 (CE-5), China's first extraterrestrial sample return mission, will be launched to the Moon in 2019, with a planned landing area near Mons Rümker in Oceanus Procellarum (Di et al., 2018b). CE-5 will collect approximately 2 kg of lunar regolith and rock samples, during which a lunar regolith core with a minimum penetration depth of 2 m will be drilled (Zhang and Ding, 2017; Tang et al., 2018). Therefore, studying the characteristics of the shallow surface of the landing area prior to mission launch will be valuable for planning sample collection and related scientific research.

Using the pictures transmitted by Luna 9, Gault et al. (1966) first identified a surficial layer of unconsolidated fragmental material on the lunar surface, which was subsequently named 'lunar regolith' (Shoemaker et al., 1967). Based on television observations and in situ measurements, lunar regolith was further strictly defined as a thin layer of fragmental material with relatively low cohesion (Oberbeck and Quaide, 1968; Shoemaker et al., 1969). The formation and evolution of lunar regolith are closely related to impacts, although volcanic ash (McKay et al., 1991) and thermal fatigue (Delbo et al., 2014; Molaro et al., 2015; Molaro et al., 2017) have also been suggested as contributors to the process. In related studies (e.g., Shoemaker et al., 1969; Gault, 1970; Oberbeck et al., 1973; Richardson, 2009; Hirabayashi et al., 2018), an intact area of the lunar surface was hypothesized, which was subsequently bombarded by both large and small impacts. As a result, a layer of fragmented, broken, melted, and agglutinated debris was ejected and distributed over the surface of the original bedrock. However, it is important to emphasize that the blanket of

* Corresponding author at: P. O. Box 9718, Datun Road, Chaoyang District, Beijing 100101, China.
E-mail address: liuzq@radi.ac.cn (Z. Liu).

https://doi.org/10.1016/j.icarus.2019.03.032
Received 14 August 2018; Received in revised form 14 March 2019; Accepted 21 March 2019
Available online 29 March 2019
0019-1035/

fragmented ejecta associated with large, individual craters on the Moon is not the same as regolith (Shoemaker et al., 1969; Melosh, 1989). The blanket ejected from individual impacts or a certain number of impacts may include large rock blocks and have an internal structure, and was named mega-regolith by Hartmann (1973). More general regolith, by contrast, is formed through an extremely large number of impact craters reaching an equilibrium state, in which small craters always reach equilibrium earlier than large craters (e.g., Gault, 1970; Richardson, 2009; Hirabayashi et al., 2017). Therefore, the surficial fragmented layer has been repeatedly disturbed and further broken into much more than the ejecta blanket substrate (Shoemaker et al., 1969; Gault, 1970; Hirabayashi et al., 2018). Under this consideration, lunar regolith is fundamentally different from the crater ejecta blanket, e.g., it is characterized as profoundly fractured and mixed (Melosh, 1989; Gault et al., 1974). Therefore, it is generally fine-grained debris with a much lower cohesive strength than the substrate (Oberbeck and Quaide, 1968).

There are several methods to estimate the depth of lunar regolith (see reviews by Wilcox et al., 2005; Fa et al., 2014; Di et al., 2016). The main method has been through the study of small crater (< 250 m) morphology (Wilcox et al., 2005). After the initial conceptual proposal, the method has been verified through laboratory experiments. There is some opposition to this method (Wilcox et al., 2005; Fa et al., 2014); therefore, a brief review of the method and its applicability is provided before we describe its implementation in this work. Together, the review and application provide knowledge of the lunar regolith in the CE-5 landing area, which is derived from rigorous analysis. We believe that the information regarding the lunar regolith thickness provided will contribute to the CE-5 mission and help provide fundamental estimates for related scientific study.

2. Crater morphology method

The basic philosophy behind the crater morphology method is that the existence of a lunar regolith layer overlying a relatively more coherent substratum would produce craters with unique morphologies (Oberbeck and Quaide, 1967; Quaide and Oberbeck, 1968). Through extensive laboratory studies, Oberbeck and Quaide (1968) identified four types of morphologies, i.e., normal, flat-bottomed, central mound, and concentric, which formed depending on the ratio D_A/t (where D_A is actually the rim-to-rim crater diameter although it has been mistaken as the apparent diameter in some previous research (e.g., Senft and Stewart, 2007; Bart, 2014), and t is the thickness of the surface). Quaide and Oberbeck (1968) also demonstrated that the position of the material boundaries for the described four crater types were almost unaffected by impact velocity, angle of impact, projectile properties, or magnitude of the gravity field within uncertainties. In addition, over much broader impact conditions (e.g., impact velocity up to 17 km/s), Senft and Stewart (2007) reproduced the same morphological variations through numerical simulation by modeling a weak regolith overlying competent rock. Therefore, the statistical distribution of the lunar regolith thickness in an area can be determined by inverting this relationship. Notably, however, Wilcox et al. (2005) raised some concerns regarding this method, such as the strength discontinuity between the surficial layer and substrate in the laboratory, and Oberbeck (2008) provided an appropriate response.

In previous studies, the method of counting all fresh small craters and identifying their morphologies has been used. However, using this method for the large area (413.8 km × 121.4 km, see Section 3 for more details) of the CE-5 is time-consuming and difficult because too many small craters need to be counted. For example, Fa et al. (2014) counted 378,556 impact craters with diameters from 4.2 to 249.8 m in Sinus Iridum (249.29 km diameter), which cost more than one year of work time (personal communication). In addition, Di et al. (2016) proposed to measure the regolith thickness directly by first modeling the pre-impact ground surface and then measuring the distance between the modeled ground surface and the crater floor or bench. However, high-precision topographic data (e.g., stereo images or derived DEM) are required. Such data sets are not available for the area of CE-5, so the method is not applicable in this research. As a result, we adopt another method by identifying only concentric craters and deriving the lunar regolith thickness through the relationship between the ratios of D_F/D_A and D_A/t (where D_F is proposed by Oberbeck and Quaide (1968) as the diameter of the floor of the flat-bottomed craters and as the diameter of the inner ring in concentric craters, and proposed by Bart (2014) as the diameter of the inner mound). The relationship was also demonstrated by Quaide and Oberbeck (1968), and it was first used by Bart et al. (2011) to survey lunar regolith depths over a large area. Later, Bart (2014) conducted more rigorous analyses of the parameters in this relationship to understand the relationship more fully. That work is the foundation of the analysis presented in this study, measuring the parameters of both D_F and D_A. This method doesn't need to identify and measure the small normal craters, which account for > 72% of the total craters described in Fa et al. (2014), thus it can save much time and effort.

As Quaide and Oberbeck (1968) and Bart et al. (2011) demonstrated, the regolith thickness is given by:

$$t = (k - D_F/D_A)D_A \tan(\alpha)/2 \quad (1)$$

where k is an empirically determined constant (0.86) and α is the angle of repose of the material (31°). The parameters in the equation were accurately defined by Bart (2014) using high-resolution images, which were also adopted in this research. High resolution images in the CE-5 landing area from the Lunar Reconnaissance Orbiter (LRO) narrow-angle camera (NAC) were used, which are the highest resolution images in this area and provide the most reliable results.

Although the method based on the morphology of small impact craters has provided useful tools for estimating regolith depth, an important issue was generally ignored in related research, that is, the possibility that impact conditions other than the particular subsurface stratigraphic structure can produce central mound, flat bottomed, or concentric craters. Kumar et al. (2011) reported that clustered impacts with low velocity can also generate central mound or flat floor craters in the Mare Imbrium, which was supported by laboratory studies of Schultz and Gault (1985). Therefore, to use crater morphology to estimate lunar regolith depth, this type of crater must be excluded. Although secondary central mound and flat floor craters can be distinguished in clusters, chains, and loops, misinterpretation is inevitable because of the primary use of subjective judgement. As a result, it is might be more optimal to perform a more conservative method, using only concentric craters to estimate lunar regolith thickness. It is necessary to note that concentric craters can also be formed provided a weak layer overlies a more resistant rock unit at depth (Melosh, 1989; Bart, 2014), but this still indicates the existence of a stratum that can be easily distinguished from lunar regolith.

In this research, we still mapped the central mound and flat-bottomed craters and also applied the above relationship to derive lunar regolith thickness. We also compared the ratio of D_F/D_A in Eq. (1) between different sources of data, which is the most sensitive factor in estimating lunar regolith (Bart, 2014). The reasons for this comparison include (1) testing whether or not central mound craters are applicable in this area; (2) providing a strategy for selecting suitable craters in other similar studies.

3. Data

The planned CE-5 landing area covers 49°W–69°W and 41°N–45°N, or roughly 443.7 km × 121.4 km. As of December 2017, there were 2299 NAC images within or overlapping this area. We selected 765 images with good quality, similar incidence angles (40°–80°), and similar resolutions. The EDR level NAC images were downloaded from the PDS website and were pre-processed with Integrated System for

Imagers and Spectrometers (ISIS) to attach the SPICE kernels (NAIF, 2014) with the "spiceinit" command; radiometric corrections were performed with the "lronaccal" command; and echo effects were removed with the "lronacecho" command.

We developed a systematic method and procedure for large-area seamless digital orthophoto map (DOM) generation and produced a high-resolution and precise DOM of the Chang'E-5 landing area (Di et al., 2018a, 2018b). First, the landing area was subdivided into 10 subareas, and a planar block adjustment with a rational function model was used to reduce the geometric inconsistencies within each subarea, and tying the images to the reference SLDEM2015 digital elevation model (DEM). The SLDEM2015 is a lunar DEM generated by co-registering and combining SELENE TC DEM with LRO laser altimetric data (Barker et al., 2016). Then, a seamless DOM mosaic was generated for each subarea. Next, a thin plate spline model based image registration was subsequently conducted on the subarea DOMs to produce a seamless DOM product for the entire landing area. A more detailed description of the method and procedure for seamless DOM generation can be found in Di et al. (2018a, 2018b). The resultant seamless DOM mosaic has a spatial resolution of 1.5 m.

4. Concentric crater mapping

Concentric craters are characterized by double annular patterns or a crater-within-crater structure (Oberbeck and Quaide, 1967), which is usually identified from shadows. For example, Fig. 1A is a typical fresh concentric crater. The shadows of the west wall are cast onto the crater interior, while the inner crater rim protruding from the shadows indicates that it is higher than the surroundings. To delineate the crater rim, the DOM mosaic was integrated into the platform of ArcGIS, and the CraterTools toolkit (Kneissl et al., 2011) was used. For each concentric crater, both the outer and inner crater rims are delineated according to the definition of Bart (2014). However, some inner crater rims are not perfectly circular (Fig. 1B), and an approximate circle is usually delineated with CraterTools. The inner crater rim is measured at the base of the crater walls as suggested in Bart (2014). CraterTools can also work well where a part of the inner crater rim is obscured or even absent (Fig. 1C). In addition, some concentric craters may also include a central mound (Fig. 1D), in which only the inner crater rim was measured and then used in this study. All the inner and outer crater diameters can be correctly determined with regard to the map projection (Kneissl et al., 2011) and subsequently used to derive the lunar regolith thickness.

5. Results

A total of 958 fresh concentric craters are identified in the CE-5 landing area. Craters are uniformly distributed over the region (Fig. 2A), and their information and the derived thickness of the lunar regolith are compiled in Table S1 in the Supporting Information. The derived lunar regolith depths range from 0.74 m to 18.00 m, with a mean of 7.15 m in this area. Fig. 2B is the median regolith thickness map from Fig. 2A, which provides a general impression of the areal distribution of the lunar regolith thickness. As observed in Fig. 2, there are substantial regional variations in regolith thickness, with much lower median regolith thickness over the southeastern region.

Fig. 3 shows a histogram of the estimated thickness in the area. Most concentric craters (~86.01%) reflect a thickness of < 10.0 m. However, there are only 7.62% (73 concentric craters) and 0.10% (1 concentric crater, Fig. S1) exhibits thickness of < 4.0 m and 2.0 m, respectively. A total of 9 concentric craters, or 0.94%, of all concentric craters indicate a lunar regolith thickness > 15.0 m, and the largest estimated lunar

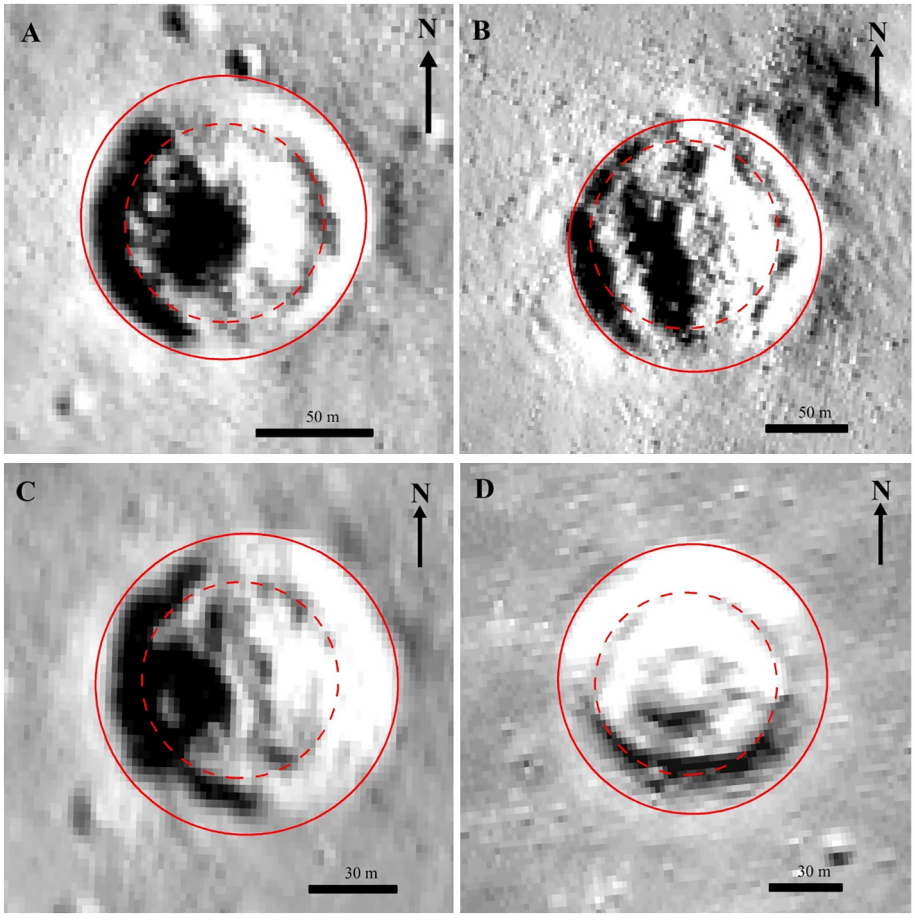

Fig. 1. Concentric crater delineation using CraterTools. (A) A typical concentric crater (59.69°W, 44.23°N) with perfect outer and inner crater rims. (B) A concentric crater with an irregular inner crater rim (65.86°W, 43.06°N). (C) A concentric crater with a partially obscured inner crater rim (61.31°W, 42.98°N). (D) A concentric crater (50.52°W, 42.94°N) with a central mound, which is also measured.

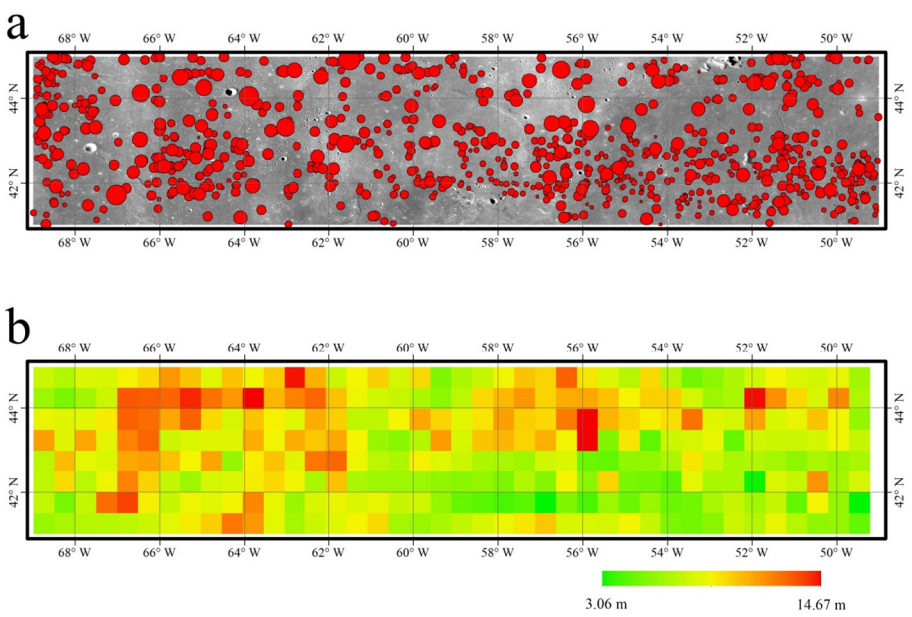

Fig. 2. Distribution of concentric craters and median regolith thickness over CE-5 landing area. (A) concentric craters and derived thickness of lunar regolith; the size of the dots are scaled with the thickness of lunar regolith from 0.74 m to 18.00 m. (B) lunar regolith thickness map derived using the natural neighbor interpolation method for every 15 km × 15 km in the CE-5 landing area.

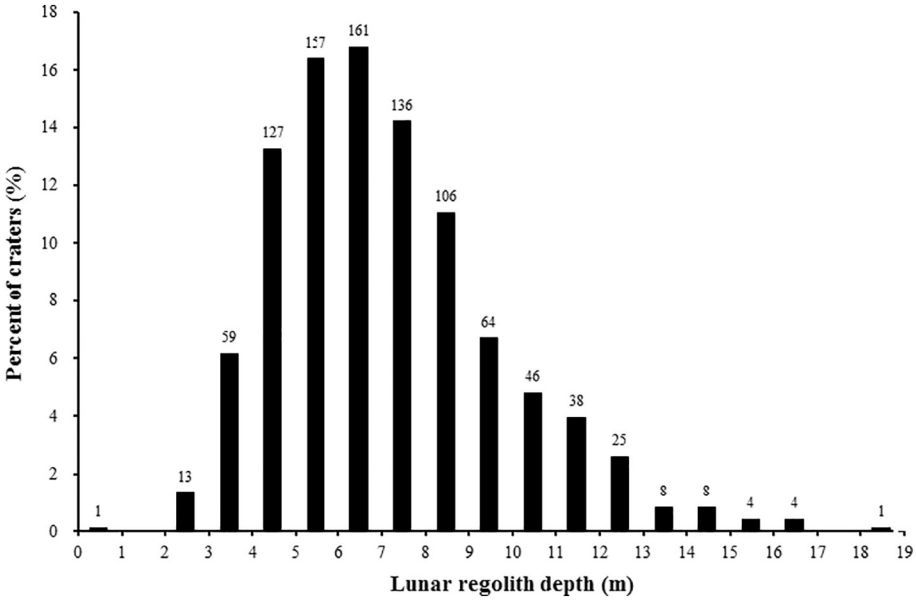

Fig. 3. Histogram of lunar regolith thickness in the planned CE-5 landing area. The horizontal axis is the thickness of lunar regolith and the vertical axis is the percentage of concentric craters indicating that thickness. The numbers above each bar is the number of the concentric craters.

Table 1
A comparison of regolith thickness estimates from previous studies with those from this work.

Thickness (m)	Method	Reference[a]
4.8 ± 1.6	Earth-based 70-cm Arecibo radar	Shkuratov and Bondarenko (2001)
4.2 ± 1.5	CE-1 microwave radio meter	Fa and Jin (2010)
7.2 ± 1.9	Dielectric constant model	Kobayashi et al. (2010)
9.04	Back propagation neural network	Meng et al. (2014)
7.15 ± 2.59	Crater morphology	This study

[a] Referred to the mean thickness in Oceanus Procellarum.

regolith thickness is 18.00 m (Fig.S2).

6. Discussion

6.1. Uncertainties in regolith thickness

Concentric craters are delineated through three points, and the standard deviation in identifying the rim points can be considered equal in both the x- and y-directions, i.e., $\sigma_x = \sigma_y = \sigma$ in this work. The crater rim is fit with the three points with the described uncertainty, and the uncertainties of the center and radius of the fit circle can be deduced according to conventional error propagation (Ghilani, 2010).

Given three points with their coordinates, i.e., a (x_a, y_a), b (x_b, y_b), and c (x_c, y_c), the fit circle can be uniquely determined. Assuming the center of the fit circle is at (x_o, y_o), the radius is r, and the angles of the triangle ABC are A, B, and C, at vertices a, b, and c, respectively. The uncertainties in the center and radius of the fit circle are:

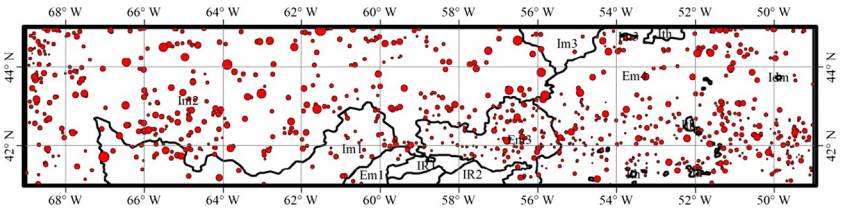

Fig. 4. Concentric crater distribution over different geologic units in the CE-5 landing area. Only the areas for the five geologic units described in the text, Em4, Em3, Im3, Im2, and Im1, have at least five concentric craters for analysis.

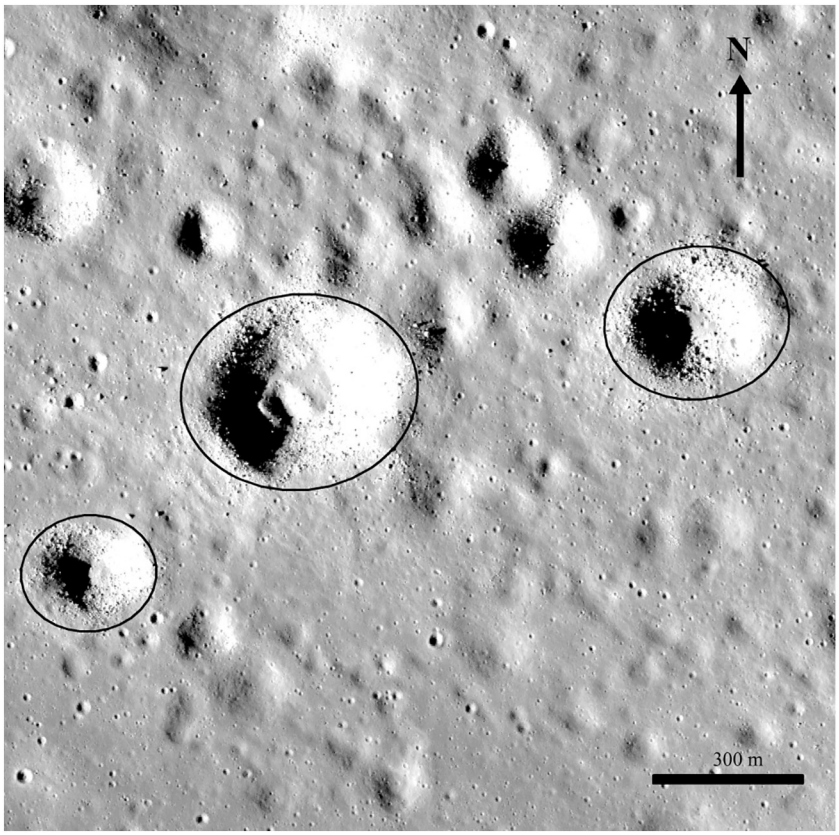

Fig. 5. Three central mound craters in the CE-5 landing area (center location is 65.23°W, 44.42°N), which are possibly from secondary impacts.

$$\sigma_{x_o} = \sigma_{y_o} = \frac{\sqrt{\sin^2 A + \sin^2 B + \sin^2 C}}{2\sqrt{2}\sin A \sin B \sin C}\sigma \tag{2}$$

$$\sigma_r = \frac{\sqrt{\sin^2 2A + \sin^2 2B + \sin^2 2C}}{4\sin A \sin B \sin C}\sigma \tag{3}$$

The detailed derivation is trivial, and the results indicate that the uncertainty is irrelevant to the size of the circle but is instead related to the distribution of the selected three points. Because CraterTools does not save the coordinates of the three points A, B, and C, these uncertainties cannot be calculated for each fit circle. However, the three points delineating the crater rim are generally evenly distributed, as requested in CraterTools (Kneissl et al., 2011), which means that A, B, and C are considered to be 60°. As a result, $\sigma_{x_o} = \sigma_{y_o} = \sqrt{\frac{2}{3}}\sigma$, and $\sigma_r = \sqrt{\frac{1}{3}}\sigma$.

In addition, uncertainties in deriving lunar regolith thickness result from Eq. (1), once again using conventional error propagation (Ghilani, 2010):

$$\sigma_t = \pm\sqrt{\left(\frac{\partial t}{\partial D_F}\sigma_{D_F}\right)^2 + \left(\frac{\partial t}{\partial D_A}\sigma_{D_A}\right)^2} \tag{4}$$

Eq. (4) can be solved with partial differential substitution and with the following equation:

$$\sigma_{D_F} = \sigma_{D_A} = \sqrt{2}\sigma_r \tag{5}$$

Therefore, the uncertainty in the lunar regolith thickness can be expressed as the following equation:

$$\sigma_t = \frac{1}{\sqrt{6}}\tan(\alpha)\sqrt{1 + k^2}\sigma \tag{6}$$

If the parameters are adopted as above ($\alpha = 31^\circ$, and $k = 0.86$), the equation will become $\sigma_t = 0.324\sigma$. In identifying the rim points, a half-pixel can be considered as the best situation that we can achieve, i.e., $\sigma = \pm 0.75$ m, which results in an uncertainty of $\sigma_t = \pm 0.24$ m.

An additional uncertainty results from the coefficients in Eq. (1). Fa et al. (2014) reanalyzed the experimental results in Quaide and Oberbeck (1968) and made a modification to the coefficients to Eq. (1) as follows:

$$t = \frac{1}{\beta}(k \pm \Delta k - D_F/D_A)D_A\tan(\alpha) \tag{7}$$

where $\beta = 1.875$, $k = 0.834$, and $\Delta k = 0.067$. We also calculate the lunar regolith thickness for reference according to the equation. The results are included in Table S1.

In addition, Bart (2014) pointed out that the optimal values for the ratio of D_F/D_A in Eq. (1) are between 0.2 and 0.7 to obtain reliable results. We found that there are 15.66% (or 150) concentric with ratios larger than 0.7, while there are no craters with ratios < 0.2. The ratio is

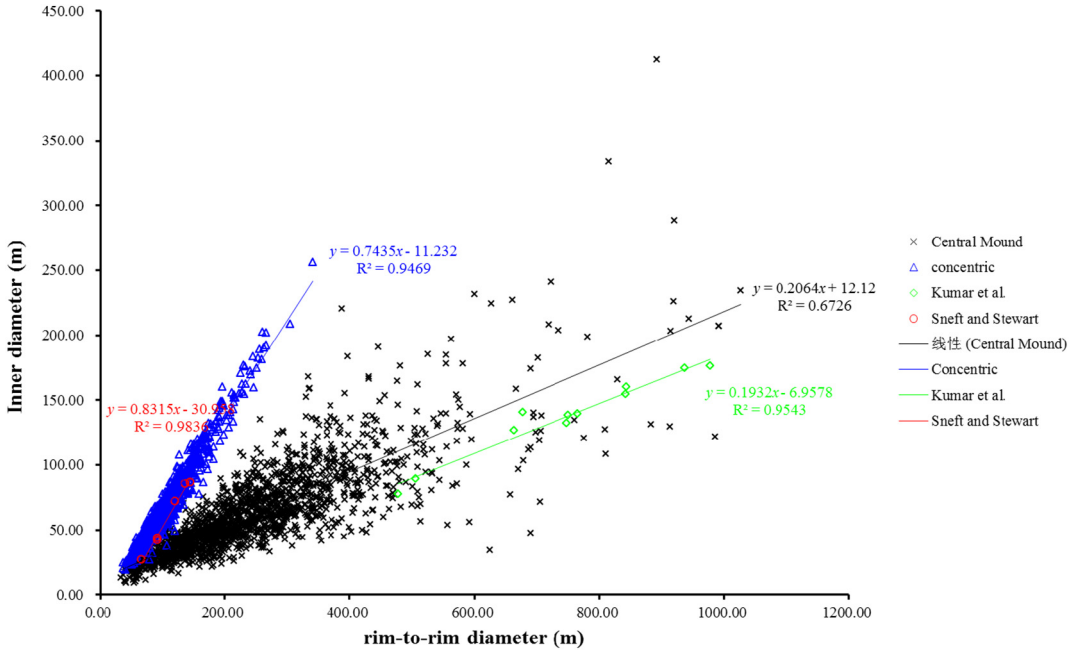

Fig. 6. Relationship between rim-to-rim diameter and inner diameter for different classes of craters. Central mound and concentric craters are mapped in this study in the CE-5 landing area. The craters measured by Kumar et al. (2011) are central mound craters from clustered projectiles, and the craters from Senft and Stewart (2007) formed in layered targets with parameters measured by Bart (2014).

also included in Table S1 for reference.

Another uncertainty in the interpretation of the results is from the methodology. Because this method is based on the strength difference between overlying fragments and the substrate layer, the measured thickness may be the thickness of the fragment layer overlying strong material if such scenario occurred in this area (see analyses by Senft and Stewart, 2007 and proposed models by Wilcox et al., 2005). Therefore, caution must be paid, especially in interpreting very low values of thickness, although we currently cannot find evidence of the existence of such strong layers.

6.2. Comparisons with other studies

According to the results from 958 concentric craters, the mean regolith thickness in the CE-5 landing area is estimated at 7.15 m, with a standard deviation of 2.59 m. The 25- and 75-percentile of the results are 5.27 m and 8.50 m, respectively. Currently, there is no other published research focused on the lunar regolith thickness in this area, and we can only compare our results with those from Oceanus Procellarum. Table 1 compares the regolith thickness in Oceanus Procellarum derived from different methods. As clearly shown, our estimation is within the ranges of the previous results and closest to that of Kobayashi et al. (2010). This comparison should be used with caution considering the values were not obtained from the same area, and the lunar regolith thickness varies significantly over small distances. In addition, there is also a large gap in the resolution of different data sources. However, this comparison is still significant because our results are similar in magnitude with other results. Because regolith thickness is estimated using the principle of concentric crater formation, based on laboratory experiments, and our study used very high-resolution images, we have confidence that our results provide reliable information on the lunar regolith thickness in the CE-5 landing area.

6.3. Lunar regolith thickness and geologic time

Lunar regolith thickness is closely related to the age of the lunar surface, and thicker regolith usually signifies older age (McKay et al., 1991). Recently, Qian et al. (2018) conducted detailed geological mapping following the assumption of Hiesinger et al. (2010) that spectrally and compositionally homogeneous areas are contained in one geologic unit. In dividing geologic units, Qian et al. (2018) analyzed topography, geomorphology and composition in this area, and as a result, 10 geologic units were defined in the CE-5 landing area. Four additional geologic units in their research were excluded because they included a slightly larger study area. We incorporated the 10 geologic units and derived ages in our study (Fig. 4). Em4 (1.21 Ga; Em refers to Eratosthenian-aged mare units, see Qian et al., 2018), Em3 (1.51 Ga), Im3 (3.16 Ga; Im refers to Imbrian-aged mare units, see Qian et al., 2018)), Im2 (3.39 Ga), and Im1 (3.42 Ga) have at least five concentric craters. Generally, lunar regolith thickness increases with geologic time among these geologic units, although there are large uncertainties due to the complexity of lunar regolith evolution.

6.4. Central mound craters in the CE-5 landing area

Central mound craters can be formed in layered targets (Quaide and Oberbeck, 1968). However, they can be also formed by clustered projectiles (Kumar et al., 2011). If most central mound craters are formed through the latter scenario, they cannot be used to estimate lunar regolith depth. In this research we mapped all the central mound craters in the CE-5 landing area, which also include a few flat floor craters. The flat floor craters are usually considered as one group, as previously indicated (e.g., Quaide and Oberbeck, 1968; Fa et al., 2014). Information about the central mound craters can be found in Table S2 in the Supporting Information.

Secondary craters can be distinguished from their distribution and morphologies in some cases. Fig. 5 shows three neighboring central mound craters, and the fitted ellipses overlying their rims have similar axis ratios and azimuths. The rocks around them indicate that their ages are not significantly different, and they are possibly originated from secondary impacts. However, this deduction is subjective and difficult to confirm in some cases, while an in-depth analysis is out of the range of this research. Because this research focuses on the lunar regolith depth calculated using Eq. (1), in which the derived lunar regolith thickness is influenced by the ratio of rim-to-rim diameter to inner diameter, the relationship between the rim-to-rim diameter and inner

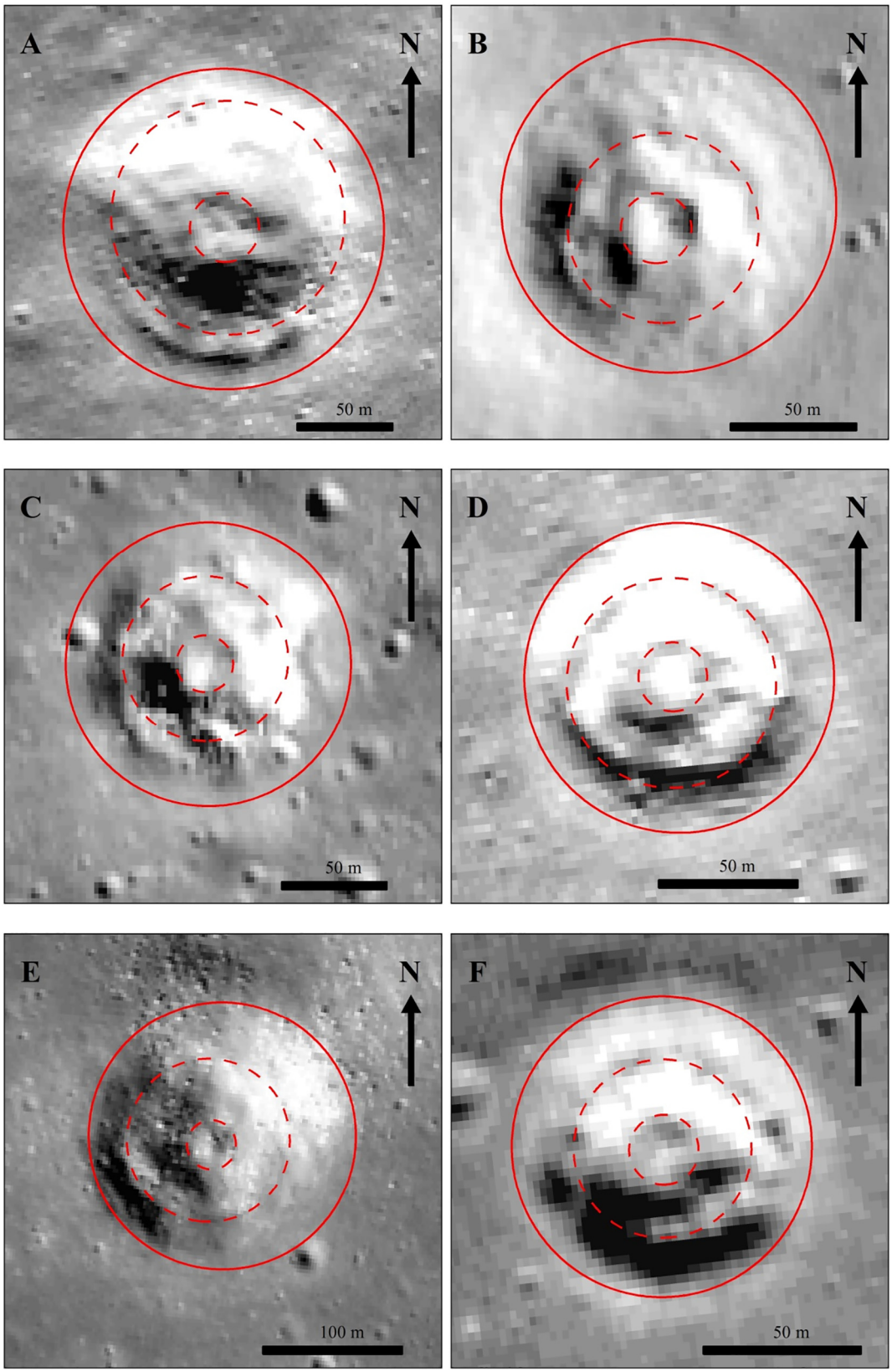

Fig. 7. Concentric craters with multi-rings. Crater D is also shown as Fig. 1D. The information of these craters is listed in Table 2.

diameter (central mound or flat floor diameter) of the 1695 central mound craters are analyzed (Fig. 6). Fig. 6 includes our derived concentric crater data, simulated craters results formed in layered targets by Senft and Stewart (2007) with parameters measured by Bart (2014), and central mound craters from clustered projectiles (Kumar et al., 2011). Notably, the central mound and flat floor craters were also included in the simulated craters Senft and Stewart (2007). Fig. 6 indicates that central mound craters mapped in the CE-5 landing area are

Table 2
Information for the multi-ring craters in Fig. 7. D_{F1} and D_{F2} are the diameters of the middle circle and inner-most circle in Fig. 7, and $Result_1$ and $Result_2$ are their derived results, respectively.

Craters in Fig. 7	Location (°)	*Da* (m)	D_{F1} (m)	D_{F2} (m)	$Result_1$ (m)	$Result_2$ (m)
A	(−50.00, 44.99)	169.14	123.17	36.01	6.69	32.88
B	(−61.93, 43.45)	133.22	75.82	28.00	11.64	26.01
C	(−59.22, 42.02)	136.00	78.90	27.01	11.43	27.03
D	(−50.52, 42.94)	112.15	75.85	25.03	6.18	21.46
E	(−67.03, 41.71)	193.05	103.74	35.00	18.70	39.3627
F	(−49.42, 42.03)	96.12	56.94	22.02	7.73	18.2253

very similar to those craters from clustered projectiles and clearly differ from the concentric craters and simulated craters in layered targets. Furthermore, using the parameters from the central mound craters to derive lunar regolith thickness in the study area would result in a mean value of 44.56 ± 28.06 m (the histogram is shown in Fig. S3), which is much higher than those compiled in Table 1. The large difference and substantial inherent standard deviation indicates that a significant number of central mound craters cannot be used to estimate lunar regolith thickness in the CE-5 landing area. Moreover, this comparison proves that concentric craters in the study area are indeed formed through layered targets, which suggests that our results are reliable. The analysis demonstrates that most of the central mound craters in the CE-5 landing area are unsuitable for estimating lunar regolith thickness, although their detailed formation process need further study.

6.5. Lunar regolith and multi-interfaces deduced from concentric craters

Based on > 1000 numerical models, Prieur et al. (2018) recently showed that concentric craters can form with a strength contrast as low as a factor of 2 or the difference in cohesion is larger than a value of 50–450 kPa between the layers. They also pointed out that such low strength contrasts may not be caused by a prominent lunar regolith-mare interface. If this is the case in the shallow subsurface of the Moon, there should be multi-interfaces and the interface between the first (top) layer and second layer would be the indication of a lunar regolith. It is also possible that the crater does not penetrate the lunar regolith, although it has the concentric morphology. In the research we identified six concentric craters possibly possessing multi-interfaces (Fig. 7), and the diameters of the mapped rings and derived depths according to the diameter of the innermost circle are presented in Table 2. The derived depths are much larger than the results in this research and from other methods in Table 1. As a result, for those craters with two or more interfaces, it is reasonable to consider the shallowest layer in the subsurface as the lunar regolith, while the interfaces in the deep layers may be an indication of blanket ejecta.

6.6. Implications for CE-5 mission

The CE-5 mission is scheduled to return ~2 kg lunar regolith samples. Although the Apollo and Luna missions returned back ~382 kg lunar samples, all of those samples, except a small fraction of glass, are older than 3.7 Ga (Stöffler and Ryder, 2001). Therefore, sampling young geologic units from lunar surface would be significant, which can fill the gap for our understanding of the late-stage lunar evolution. In addition, the radiogenic isotope ages from these young samples could be used to calibrate the crater size-frequency distribution curve (Qian et al., 2018), which has been widely used in lunar and other planetary surface dating (e.g., Shoemaker et al., 1962; Stöffler and Ryder, 2001; Hiesinger et al., 2010). Therefore, we also suggest landing on the young geologic unit of Em4, as Qian et al. proposed (Qian et al., 2018).

It is significant to study the source craters of the samples returned by CE-5 before they are used for isotopic dating. A crater is generally surrounded firstly by continuous deposit of debris and then by patchy ejecta or even dispersed blocks (Melosh, 1989). Based on the results of nuclear and high explosive cratering events, small scale laboratory cratering experiments, natural meteorite impact craters, and estimates for lunar craters, numerous cratering events, McGetchin et al. (1973) found a simple relationship between the thickness of ejecta blanket and the radial range to the crater center over a wide range of scales:

$$t_e = 0.14R^{0.74}(r/R)^{-3.0} \quad (8)$$

where r is the range from the center of the crater and R is the apparent crater radius, all in meters. The equation has been used to estimate the ejecta thickness in many studies (e.g., Hörz et al., 1983; Bratt et al., 1985; Fassett et al., 2011), and it can be also used to predict the ejecta thickness from craters. The source crater of ejected boulders can be also deduced if they are not very far from crater rim (Bart and Melosh, 2010). On the other hand, it is usually difficult to derive the source craters for the distant blocks in the landing area. For example, Orientale ejecta may have been deposited over the entire moon (Moore et al., 1974; Spudis et al., 1984); however, there is no undeniable rock fragment in previous returned lunar samples and its age is also from crater size-frequency distribution model (e.g., Stöffler et al., 2006; Wilhelms et al., 1987; Stöffler and Ryder, 2001; Whitten et al., 2011). Recently, based on the distribution of impact events and cratering process, Liu et al. (2019) created a model to predict regolith mixing by impacts and demonstrated its reliability through predicating the occurrence of impact melt in Apollo and Luna sampling spots from distant basins, which can shed light on solving the problem.

The plan is for CE-5 to drill a core at a minimum depth of 2 m (Zhang and Ding, 2017; Di et al., 2018b; Tang et al., 2018), which would be facilitated by a lunar regolith is thicker than 2 m. As can be seen from our results, the thickness of lunar regolith in Em4 is > 3 m; thus, it is enough for CE-5 to drill a 2-m core. Another consideration is the probability of encountering blocks during the core-drilling, which can be analyzed according to the ratio of the influence area calculated from all particles large enough to interfere with the penetrating probe to the total area (Mitchell et al., 1971). This probability depends on both the size of the blocks and the diameter of the probe, which can be derived if ground images are obtained before operation. However, similar operations by Apollo 15 (a 2.4-m core near the landing site, Mitchell et al., 1972a), Apollo 16 (a 2.34-m core in the Apollo lunar surface experiment area, Mitchell et al., 1972b), and Apollo 17 (a deep core to a depth of 3.05 m at approximately 40 m north of the Apollo lunar surface experiment area, Mitchell et al., 1973) were successfully performed.

7. Conclusions

In this study, we investigated the lunar regolith thickness in the CE-5 landing area using a crater morphology method. Considering that some central mound and flat floor craters can be formed from clustered impacts, only concentric craters were used to calculate regolith depth in this study. Our results indicate that the lunar regolith in this area ranges from 0.74 m to 18.00 m in thickness, with a mean of 7.15 m. Lunar regolith is generally thinner in the southeast study area but remains thicker than 2 m over most of the CE-5 landing area. There are 73 concentric craters that indicate a lunar regolith < 4.0-m thick and one

that indicates a regolith thickness of < 2.0 m, suggesting that the coherent substratum is relatively shallow. This observation should be considered during the CE-5 sample retrieval.

Supplementary data to this article can be found online at https://doi.org/10.1016/j.icarus.2019.03.032.

Acknowledgements

The authors gratefully acknowledge Arizona State University for providing LRO NAC images. The authors also thank Thomas Kneissl for the software CraterTools and two anonymous reviewers for their suggestions. This work was supported by the Key Research Program of the Chinese Academy of Sciences (Grant No. XDPB11) and National Natural Science Foundation of China (Grant No. 41490635 and 41590851).

References

Barker, M.K., Mazarico, E., Neumann, G.A., Zuber, M.T., Haruyama, J., Smith, D.E., 2016. A new lunar digital elevation model from the Lunar Orbiter Laser Altimeter and SELENE Terrain Camera. Icarus 273, 346–355.
Bart, G.D., 2014. The quantitative relationship between small impact crater morphology and regolith depth. Icarus 235, 130–135.
Bart, G.D., Melosh, H.J., 2010. Distributions of boulders ejected from lunar craters. Icarus 209, 337–357.
Bart, G.D., Nickerson, R.D., Lawder, M.T., Melosh, H.J., 2011. Global survey of lunar regolith thickness from LROC images. Icarus 215 (2), 485–490.
Bratt, S.R., Solomon, S.C., Head, J.W., Thurber, C.H., 1985. The deep structure of lunar basins: implications for basin formation and modification. J. Geophys. Res. 90, 3049–3064.
Delbo, M., Libourel, G., Wilkerson, J., Murdoch, N., Michel, P., Ramesh, K.T., Ganino, C., Verati, C., Marchi, S., 2014. Thermal fatigue as the origin of regolith on small asteroids. Nature 508 (7495), 233–236.
Di, K., Sun, S., Yue, Z., Liu, B., 2016. Lunar regolith thickness determination from 3D morphology of small fresh craters. Icarus 267, 12–23.
Di, K., Jia, M., Xin, X., Liu, B., Liu, Z., Peng, M., Yue, Z., 2018a. High resolution seamless mapping of Chang'E-5 landing area using LROC NAC images. Lunar Planet. Sci. Conf. 49 (abstract 1752).
Di, K., Jia, M., Xin, X., Liu, B., Liu, Z., Pang, M., Yue, E., 2018b. High resolution seamless DOM generation over Chang'E-5 landing area using LROC NAC images. In: Int. Arch. Photogramm. Remote Sens. Spatial Inf. Sci., XLII-3, pp. 271–276.
Fa, W., Jin, Y.-Q., 2010. A primary analysis of microwave brightness temperature of lunar surface from Chang-E 1 multi-channel radiometer observation and inversion of regolith layer thickness. Icarus 207 (2), 605–615.
Fa, W., Liu, T., Zhu, M.-H., Haruyama, J., 2014. Regolith thickness over Sinus Iridum: results from morphology and size-frequency distribution of small impact craters. J. Geophys. Res. Planets 119, 1914–1935.
Fassett, C.I., Head, J.W., Smith, D.E., Zuber, M.T., Neumann, G.A., 2011. Thickness of proximal ejecta from the Orientale Basin from Lunar Orbiter Laser Altimeter (LOLA) data: implications for multi-ring basin formation. Geophys. Res. Lett. 38, L17201.
Gault, D.E., 1970. Saturation and equilibrium conditions for impact cratering on the lunar surface: criteria and implications. Radio Sci. 5, 273–291.
Gault, D.E., Quaide, W.L., Oberbeck, V.R., Moore, H.J., 1966. Luna 9 photographs: evidence for a fragmental surface layer. Science 153, 985–988.
Gault, D.E., Hörz, F., Brownlee, D.E., 1974. Mixing of the lunar regolith. Proc. Lunar Planet. Sci. Conf. 3, 2365–2386.
Ghilani, C.D., 2010. Adjustment Computations: Spatial Data Analysis. John Wiley & Sons, Incorporation, New Jersey.
Hartmann, W.K., 1973. Ancient lunar mega-regolith and subsurface structure. Icarus 18, 634–636.
Hiesinger, H., Head III, J.W., Wolf, U., Jaumann, R., Neukum, G., 2010. Ages and stratigraphy of lunar mare basalts in Mare Frigoris and other nearside Maria based on crater size-frequency distribution measurements. J. Geophys. Res. 115, E03003.
Hirabayashi, M., Minton, D.A., Fassett, C.I., 2017. An analytical model of crater count equilibrium. Icarus 289, 134–143.
Hirabayashi, M., Howl, B.A., Fassett, C.I., Soderblom, J.M., Minton, D.A., Melosh, H.J., 2018. The role of breccia lenses in regolith generation from the formation of small, simple craters: application to the Apollo 15 landing site. J. Geophys. Res. 123, 527–543.
Hörz, F., Ostertag, R., Rainey, D.A., 1983. Bunte Breccia of the Ries: continuous deposits of large impact craters. Rev. Geophys. 21, 1667–1725.
Kneissl, T., van Gasselt, S., Neukum, G., 2011. Map–projection–independent crater size-frequency determination in GIS environments–new software tool for ArcGIS. Planet. Space Sci. 59 (11 − 12), 1243–1254.
Kobayashi, T., Kim, J.H., Lee, S.R., Araki, H., Ono, T., 2010. Simultaneous observation of lunar radar sounder and laser altimeter of Kaguya for lunar regolith layer thickness estimate. IEEE Geosci. Remote Sens. Lett. 7 (3), 435–439.
Kumar, P.S., Kumar, A.S., Keerthi, V., Goswami, J.N., Krishna, B.G., Kumar, A.S.K., 2011. Chandrayaan-1 observation of distant secondary craters of Copernicus exhibiting central mound morphology: evidence for low velocity clustered impacts on the moon. Planet. Space Sci. 59, 870–879.
Liu, T., Michael, G., Engelmann, J., Wünnemann, K., Obersta, J., 2019. Regolith mixing by impacts: lateral diffusion of basin melt. Icarus 321, 691–704.
McGetchin, T.R., Settle, M., Head, J.W., 1973. Radial thickness variation in impact crater ejecta: implications for lunar basin deposits. Earth Planet. Sci. Lett. 20, 226–236.
McKay, D.S., Heiken, G., Basu, A., Blanford, G., Simon, S., Reedy, R., French, B.M., Papike, J., 1991. The lunar regolith. In: Heiken, G., Vaniman, D., French, B.M. (Eds.), Lunar Sourcebook: A user's Guide to the Moon. CUP Archive, pp. 285–356.
Melosh, H.J., 1989. Impact Cratering: A Geologic Process. Oxford University Press, New York, pp. 197.
Meng, Z., Xu, Y., Zheng, Y., Zhu, Y., Jia, Y., Chen, S., 2014. Inversion of lunar regolith layer thickness with CELMS data using BPNN method. Planet. Space Sci. 101, 1–11.
Mitchell, J.K., Bromwell, L.G., Carrier III, W.D., Costes, N.C., Scott, R.F., 1971. Soil mechanics experiment. In: Chapman, P.K., Duke, M.B., Foley, H.N., Harris, J., Herbert, F.J., Mercer, B., Simpkinson, S.H., Stull, P.J., Ward, J.M. (Eds.), Apollo 14 Preliminary Science Report.
Mitchell, J.K., Bromwell, L.G., Carrier III, W.D., Costes, N.C., Houston, W.N., Scott, R.F., 1972a. Soil mechanics experiment. In: Allen, J.P., Anderson, K.F., Baldwin, R.R., Cox, R.L., Foley, H.N., Giesecke, R.L., Koos, R.H., Mercer, R.M., Phinney, W.C., Roberson, F.I., Simpkinson, S.H. (Eds.), Apollo 15 Preliminary Science Report.
Mitchell, J.K., Carrier III, W.D., Houston, W.N., Scott, R.F., Bromwell, L.G., Durgunoglu, H.T., Hovland, H.J., Treadwell, D.D., Costes, N.C., 1972b. Soil mechanics. In: Brett, R., England, A.W., Calkins, J.E., Giesecke, R.L., Holman, D.N., Mercer, R.M., Murphy, M.J., Simpkinson, S.H. (Eds.), Apollo 16 Preliminary Science Report.
Mitchell, J.K., Carrier III, W.D., ostes, N.C., Houston, W.N., Scott, R.F., Hovland, H.J., 1973. Soil mechanics. In: Robert, A.P., Baldwin, R.R., Brett, R., Fuller, J.D., Giesecke, R.L., Hanley, J.B., Holman, D.N., Mercer, R.M., Montgomery, S.N., Murphy, M.J., Simpkinson, S.H. (Eds.), Apollo 17 Preliminary Science Report.
Molaro, J.L., Byrne, S., Langer, S.A., 2015. Grain-scale thermoelastic stresses and spatiotemporal temperature gradients on airless bodies, implications for rock breakdown. J. Geophys. Res. 120, 255–277.
Molaro, J.L., Byrne, S., Le, J.-L., 2017. Thermally induced stresses in boulders on airless body surfaces, and implications for rock breakdown. Icarus 294, 247–261.
Moore, H.J., Hodges, C.A., Scott, D.H., 1974. Multi-ringed basins–illustrated by Orientale and associated features. Proc. Lunar Sci. Conf. 71–100 (5th).
NAIF, 2014. Lunar Reconnaissance Orbiter Camera (LROC) Instrument Kernel v18. http://naif.jpl.nasa.gov/pub/naif/pds/ data/lro-l-spice-6-v1.0/lrosp_1000.
Oberbeck, V.R., 2008. Comment on: constraints on the depth and variability of the lunar regolith, by B. B. Wilcox, M. S. Robinson, P. C. Thomas, and B. R. Hawke. Meteorit. Planet. Sci. 43 (4), 815–817.
Oberbeck, V.R., Quaide, W.L., 1967. Estimated thickness of a fragmental surface layer of Oceanus Procellarum. J. Geophys. Res. 72 (18), 4697–4704.
Oberbeck, V.R., Quaide, W.L., 1968. Genetic implications of lunar regolith thickness variations. Icarus 9, 446–465.
Oberbeck, V.R., Quaide, W.L., Mahan, M., Paulson, J., 1973. Monte Carlo calculations of lunar regolith thickness distributions. Icarus 19 (1), 87–107.
Prieur, N.C., Rolf, T., Wünnemann, K., Werner, S.C., 2018. Formation of simple impact craters in layered targets: implications for lunar crater morphology and regolith thickness. J. Geophys. Res. 123 (6), 1555–1578.
Qian, Y. Q., Xiao, L., Zhao, S. Y., Zhao, J. N., Huang, J., Flahaut, J., et al. (2018). Geology and scientific significance of the Rümker region in northern Oceanus Procellarum: China's Chang'E-5 landing region. J. Geophys. Res. Planets, 123 (6), 1407–1430.
Quaide, W.L., Oberbeck, V.R., 1968. Thickness determinations of the lunar surface layer from lunar impact craters. J. Geophys. Res. 73 (16), 5247–5270.
Richardson, J.E., 2009. Cratering saturation and equilibrium: a new model looks at an old problem. Icarus 204 (2), 697–715.
Schultz, P.H., Gault, D.E., 1985. Clustered impacts: experiments and implications. J. Geophys. Res. 90, 3701–3732.
Senft, L.E., Stewart, S.T., 2007. Modeling impact cratering in layered surfaces. J. Geophys. Res. 112, 11002.
Shkuratov, Y.G., Bondarenko, N.V., 2001. Regolith layer thickness mapping of the moon by radar and optical data. Icarus 149 (2), 329–338.
Shoemaker, E.M., Hackman, R.J., Eggleton, R.E., 1962. Interplanetary correlation of geologic time. Adv. Astronaut. Sci. 8, 70–79.
Shoemaker, E.M., Batson, R.M., Hold, H.E., Morris, E.C., Rennilson, J.J., Whitaker, E.A., 1967. Surveyor V: television pictures. Science 158, 642–652.
Shoemaker, E.M., Batson, R.M., Holt, H.E., Morris, E.C., Rennilson, J.J., Whitaker, E.A., 1969. Observations of the lunar regolith and the earth from the television camera on surveyor 7. J. Geophys. Res. 74, 6081–6119.
Spudis, P.D., Hawke, B.R., Lucey, P., 1984. Composition of Orientale basin deposits and implications for the lunar basin-forming process. J. Geophys. Res. Planet 89 (S01), C197–C210.
Stöffler, D., Ryder, G., 2001. Stratigraphy and isotope ages of lunar geologic units: chronological standard for the inner solar system. Space Sci. Rev. 96 (1–4), 9–54.
Stöffler, D., Ryder, G., Ivanov, B.A., Artemieva, N.A., Cintala, M.J., Grieve, R.A.F., 2006. Cratering history and lunar chronology. Rev. Mineral. Geochem. 60, 519–596.
Tang, J., Quan, Q., Jiang, S., Liang, J., Lu, X., Yuan, F., 2018. Investigating the soil removal characteristics of flexible tube coring method for lunar exploration. Adv. Space Res. 61, 799–810.
Whitten, J., Head, J. W., Staid, M., Pieters, C. M., Mustard, J., Clark, R., et al., 2011. Lunar mare deposits associated with the Orientale impact basin: new insights into mineralogy, history, mode of emplacement, and relation to Orientale Basin evolution from moon mineralogy mapper (M-3) data from Chandrayaan-1. J. Geophys. Res. Planet, 116, E00G09.
Wilcox, B.B., Robinson, M.S., Thomas, P.C., Hawke, B.R., 2005. Constraints on the depth and variability of the lunar regolith. Meteorit. Planet. Sci. 40 (5), 695–710.
Wilhelms, D.E., McCauley, J.F., Trask, N.J., 1987. The Geologic History of the Moon, USGS Professional Paper 1348. US Government Printing Office, Washington DC, pp. 1–281.
Zhang, T., Ding, X., 2017. Drilling forces model for lunar regolith exploration and experimental validation. Acta Astron 131, 190–203.